View metadata, citation and similar papers at core.ac.uk

brought to you by CORE

provided by Warwick Research Archives Portal Repository

Original citation:
Boscato, Giosuè, Casalegno, Carlo, Russo, Salvatore and Mottram, J. Toby (James Toby), 1958-. (2013) Buckling of built-up columns of pultruded fiber-reinforced polymer C-sections. Journal of Composites for Construction . 04013050. ISSN 1090-0268

Permanent WRAP url:
http://wrap.warwick.ac.uk/58216/

Copyright and reuse:
The Warwick Research Archive Portal (WRAP) makes this work by researchers of the University of Warwick available open access under the following conditions. Copyright © and all moral rights to the version of the paper presented here belong to the individual author(s) and/or other copyright owners. To the extent reasonable and practicable the material made available in WRAP has been checked for eligibility before being made available.

Copies of full items can be used for personal research or study, educational, or not-for-profit purposes without prior permission or charge. Provided that the authors, title and full bibliographic details are credited, a hyperlink and/or URL is given for the original metadata page and the content is not changed in any way.

A note on versions:
The version presented here may differ from the published version or, version of record, if you wish to cite this item you are advised to consult the publisher's version. Please see the 'permanent WRAP url' above for details on accessing the published version and note that access may require a subscription.

For more information, please contact the WRAP Team at: publications@warwick.ac.uk

http://wrap.warwick.ac.uk

G. Boscato, C. Casalegno, S. Russo and J. T. MOTTRAM, 'Buckling of built-up columns of pultruded FRP C-sections,' *Journal of Composites for Construction*, http://ascelibrary.org/doi/abs/10.1061/%28ASCE%29CC.1943-5614.0000453

Buckling of Built-up Columns of Pultruded FRP C-sections

Giosuè Boscato[1], Carlo Casalegno[2], Salvatore Russo[3], and J. Toby Mottram[4]

ABSTRACT

This paper presents the test results of an experimental investigation to evaluate the buckling behaviour of built-up columns of pultruded profiles, subjected to axial compression. Specimens are assembled using four (off-the-shelf) channel shaped profiles of E-glass Fibre Reinforced Polymer (FRP), having the similar detailing as strut members in a large FRP structure that was executed in 2009 to start the restoration of the Santa Maria Paganica church in L'Aquila, Italy. This church had partially collapsed walls and no roof after the 2009 April 6th earthquake of 6.3 magnitude. A total of six columns have been characterised with two different configurations for the bolted connections joining together the channel sections into a built-up strut. Test results are discussed and a comparison is made with closed form equation predictions for flexural buckling resistance, and with buckling resistances established from both Eigenvalue and geometric non-linear finite element analyses. Results reported and discussed show that there is a significant role played by the end loading condition, the composite action and imperfections. Simple closed form equations are found to overestimate the flexural buckling strength, whilst the resistance by the non-linear analysis is

[1]Ph.D., Department of Construction, IUAV University of Venice, Dorsoduro 2206, 30123 Venice, Italy. E-mail: gboscato@iuav.it
[2]Ph.D., Department of Construction, IUAV University of Venice, Dorsoduro 2206, 30123 Venice, Italy (corresponding author). E-mail: carlo.casalegno@polito.it
[3]Associate Professor of Structural Civil Engineering, Department of Construction, IUAV University of Venice, Dorsoduro 2206, 30123 Venice, Italy. E-mail: russo@iuav.it
[4]Professor, School of Engineering, University of Warwick, Coventry CV4 7AL, UK. E-mail: J.T.Mottram@warwick.ac.uk

seen to give a reasonably reliable numerical approach to establishing the actual buckling behaviour.

SUBJECT HEADINGS: Buckling, pultruded built-up columns, laboratory tests, finite element analysis

INTRODUCTION

The use of Fibre Reinforced Polymer (FRP) shapes and systems in construction has significantly increased in recent years. The increased interest lies in the advantages over traditional construction materials, such as high strength-to-weight ratio, corrosion resistance and the ease of transportation and erection (Mottram 2011).

Pultrusion is a composite manufacturing process for the continuous production of FRP thin-walled shapes. One category of Pultruded (PFRP) profiles possess the same cross-sectional shapes (I, H, Leg-angle, channel, box, etc.) as found in structural steelwork, but these standard profiles are not as large, and have very different mechanical and structural properties (Bank 2006). They consist of E-glass fibre reinforcement having layers of unidirectional rovings and continuous mats in a thermoset resin based matrix, usually of a polyester or vinylester polymer resin. Having a weight of only 25% of steel these profiles offer lightweight structural solutions. Like steel, the tensile strength in the longitudinal direction is more than 200 MPa. The longitudinal modulus of elasticity lies in the range 20-30 GPa, which is 10-6 times lower than steel. The elastic modulus in the transverse direction is 0.3 of the longitudinal value. The expected range for the in-plane shear modulus of elasticity of PFRP material is 3 to 5 GPa.

The mechanical performance of individual PFRP structural profiles for frame members has received attention by researchers (Bank 2006; Russo 2007; Boscato & Russo 2009; Boscato *et al*. 2011). This is not the situation for built-up (column) members subjected to concentric loading, and this form of member is the subject of a fact finding study reported in this paper.

The predominantly linear elastic mechanical properties of PFRP material (Bank 2006) leads to different column response because there is neither material yielding nor gross plasticity deformation. For the same cross-section dimensions the thin-walled PFRP column (of 'I' or 'H' shape) has the potential to fail first with a local instability buckling mode (Mottram 2004). Moreover, the buckling response is more related to the actual geometry of the cross-section than to the member's slenderness (however this non-dimensional column length is established). In general, PFRP columns of open-sectioned shape ('H' or 'I') will be subjected to failure by global (flexural) buckling of the member or by local (plate) buckling of the flange outstands (Barbero, Dede and Jones, 2000: Lane and Mottram 2002; Mottram, Brown and Anderson 2003).

The local instability mode causes outstands to rotate about their intersection junction with the web; this is particularly true for the wide flange (or 'H') profiles with height and breadth of same dimensions. It has been shown via experimental investigations that axially compressed H- and I-shapes can give one of two distinct types of failure, with local buckling occurring in 'shorter' columns that do not crush first, and flexural buckling prevailing when the member's effective length classify the column as 'slender'. For intermediate slendernesses the two instabilities may coexist and there might be imperfection sensitive modal coupling interaction that leads to a tertiary buckling mode. Lane and Mottram (2002) have shown from axial column tests with H-shapes that modal coupling lowers the buckling resistance by a few percent in the transition range for column lengths between the two distinct modes of elastic buckling.

Several research groups have contributed towards the development of knowledge to understand the elastic buckling response of PFRP columns of standard shapes. From the plethora of sources (refer to literature database at: www2.warwick.ac.uk/fac/sci/eng/staff/jtm/pfrp_latest.pdf) a number of investigations of note

73 are by Barbero *et al*. (2000), Pecce and Cosenza (2000), Hashem and Yuan (2001), Lane and
74 Mottram (2002), Di Tommaso and Russo (2003), Mottram (2004) and Turvey and Zhang
75 (2006). None of the previous studies involved a built-up column member and so the study
76 reported in this paper is novel and will add to what we know and understand. Because of
77 practical limitations in processing capabilities the maximum size for an 'off-the–shelve'
78 PFRP has a cross-section area of about 13000 mm^2 (for a I-profile of 610 x 178 x 12.7 mm).
79 The advantage of the built-up fabrication option is that it would allow bigger cross-sectional
80 sized members to be used in structural/civil engineering projects.
81 The structural response might be even more complex for a built-up column that is fabricated
82 from joining together (individual) standard PFRP profiles by a method of mechanical
83 fastening. Complexity could increase because of the possible interaction of buckling modes
84 within the individual shapes and the influence of composite action between them. Moreover,
85 the presence of material, geometrical and 'loading' imperfections is likely to have a influence
86 on how the built-up member responds and fails, when subjected to concentric compression
87 loading.
88 Presented in this paper are the test results from an experimental investigation to address and
89 evaluate the buckling characteristics of a PFRP built-up column. The column's detailing is
90 similar to strut members in the 1050 m^2 by 30 m high FRP structure located inside the church
91 of Santa Maria Paganica in L'Aquila (Russo, Boscato and Mottram 2012; Russo 2012). This
92 church lost its roof and parts of the masonry walls in the 6^{th} April 2009 earthquake and, until
93 government funds are available for the restoration work, its fragile interior requires protection
94 from the weather. The engineered solution formulate in 120 days (Russo *at al*. 2012) was to
95 execute a temporary structure of FRP material (and at 8 kg per m^2 it is a light weight
96 solution). To understand the measured responses the column failure results are compared

with resistances from closed form equations for flexural buckling and numerical results from Eigenvalue (bifurcation buckling) and geometrical non-linear finite element analyses.

DESCRIPTION OF BUILT-UP STRUT

The goal of this study is to investigate the structural performance of a built-up member, subjected to uniform compression, similar to those adopted in the construction of the L'Aquila FRP structure shown in Figures 1(a) and 1(b). Shown in Figure 1(b) is the structural system chosen to address the important design issues of second-order effects in ULS design and to provide a suitable configuration for the (M14 steel) bolted gusset plate joints. Frame jointing is characterized by using FRP components manufactured by two different composite processing methods. The gusset plating (for in-plane isotropic properties) seen in Figure 1(b) was manufactured using the bag molding process. The strut members are assembled from four off-the-shelf pultruded channel-shaped sections having same cross-section dimensions (152 x 43 mm) and wall thickness of 9.5 mm.

Figure 2(a) shows the tested built-up member's cross-section (envelop is 152 x 171 mm) comprising four channel (C) profiles, with two (back-to-back) for the web and two for the flanges. Connections between the channels were made using M10 (stainless) steel bolting in 1 mm clearance holes. Bolts were tightened to a torque of 45 Nm. The two Cs for the web of 6.5 mm thickness were connected using two bolts and packing plates at spacings of $1/3^{rd}$ (911 mm) and $2/3^{rd}$ (1822 mm) along the column's length (L is 2734 mm). As seen in Figure 2(a) there is a bolted connection between a flange in the web and the web of a channel for the member's flange. In column testing the compressive force is ('uniformly') applied directly into the web's two C-profiles with an area of 3000 mm^2. The two Cs forming the flanges are present to increase the built-up column's lateral flexural stiffness.

Geometrical and physical properties for the strut member are reported in Table 1. Column (1) defines the property and Column (2) gives its notation. Listed in Column (3) are the cross-section's properties (to three significant figures) for a constant ('Nominal') wall thickness of 9.5 mm in the four channels. This is the cross-section size for struts, see Figure 1, in the L'Aquila temporary structure (Russo *at al*. 2012). The equivalent properties in Column (4) are for the cross-section used in the experimental ('Exp') investigation, as it comprised three Cs of 6.5 mm thickness (two web and one flange) and one flange C with thicker walls at 9.5 mm thickness. The justification for the asymmetric cross-section about the major-axis of bending was to trigger second-order effects from onset of the compression loading.

EXPERIMENTAL INVESTIGATION

The static test configuration for the experimental investigation is illustrated in Figure 2. Figure 2(a) shows the overall column specimen, which can be with or without the third-length (at $L/3$ and $2L/3$) bolting (see Figure 2(d)) between the web and the flange Cs. It also shows that at the mid-height section there are eight axial strain gauges (SG1 to SG8) and two displacement transducers numbered [18] and [19]. Images in Figures 2(b) and 2(c) show that the hinge-hinge end condition is realized by using a steel sphere placed between 'rigid' steel plates in contact with the PFRP specimen and testing machine. A specimen is placed in the testing machine so that the centre of the cross-sections area is closely aligned with the compression load path. The end fixture allows for unrestrained global flexural or flexural-torsional instability deformation to occur.

This fact finding test series involved the two column configurations with labels CFG1 and CFG2, having three specimens per batch. CFG1 is for the built-up member with full bolting at four cross-section levels and CFG2 is for without bolting at the two 1/3rd height locations. Removal of the bolting was to facilitate the release of the composite action between the web

and flange Cs, and can be expected to expose the effectiveness of using spaced bolt rows in built-up members. Note that the equivalent bolting located close to the two free ends cannot be removed. One objective of the study was to establish the level of composite action from having made the design decision to have bolting at the 1/3rd length spacing.

Compression force was applied using a computer controlled universal testing machine of 600 tonne (6000 kN) capacity. To measure the (longitudinal) response the specimen, at $L/2$ (1367 mm), has the eight strain gauges (SG1 to SG8) shown in Figure 2(a). SG1, SG2 and SG6 are on the flange C-section of 9.5 mm thickness, whilst SG3 to SG5 are on the other flange C-section of 6.5 mm thickness. Gauges SG7 and SG8 are positioned at the centre of the two back-to-back Cs forming the the web. Measurement of lateral displacement along the Minor-axis and Major-axis planes was made using displacement transducers. Transducers [18] and [19] are located at mid-height. For the flexural deformation about the Minor-axis there is third transducer, labeled [20], that is located at $L/4$ (684 mm) (see Fig. 2(a)). Because the half-wave length(s) for potential local instabilities was unknown no transducers were involved with the requirement to pick-up deformation signaling local buckling failure. The origin for the length of the column specimen is at the base of the specimen.

Test Results

Results for the two column configurations of CFG1 and CFG2 are plotted in Figures 3 to 8. Figures 3 to 5 are for the three CFG1 specimens, whilst Figures 6 to 8 are for the three CFG2 columns. In each of the figures, part (a) reports, at $L/2$, the axial strains from SG1 to SG 8, and part (b) gives the lateral displacements at $L/4$ from [20] and at $L/2$ from [18] and [19] for the Major axis and Minor axis components. The plot axes are the same in part (a) for the compressive strain and average compressive stress (with σ positive), calculated using the (mid-height) cross-section area A from Column (4) in Table 1. The compressive stress given

171 in the figures is for the axial compression load alone. It does not therefore represent the
172 highest fiber compression stress due to the combination of axial and flexural deformations.
173 Because the flexural deformation can occur in two directions about the principal axes the
174 abscissa axis in part (b) of Figures 3 to 8 is specific to the test. To highlight the load carrying
175 capacity of the columns the ordinate axis in part (b) is for the applied compression force.
176 The eight strain gauge readings in Part (a) of Figures 3 to 5 show that the CFG1 cross-section
177 in tests 1 to 3 is initially compressed with a fairly uniform compressive stress. Significant
178 divergence between the eight stress-strain curves is recorded when the load exceeds 55 kN
179 (or 8.3 MPa) in test 1 (Figure 3), 117 kN (or 17.8 MPa) in test 2 (Figures 4) and 78 kN (or
180 11.8 MPa) in test 3 (Figure 5). Below this transition state the difference between the
181 minimum and maximum strains is 52%, 47% and 36% respectively. Afterwards the presence
182 of deformations associated with individual-section flexural buckling and/or built-up member
183 flexural buckling radically alters a column's response. This behavior causes a sudden
184 increase in the difference between the minimum and maximum strains to 86%, 80% and 83%.
185 The main difference in response is observed by a relatively higher increase in the SG7 and
186 SG8 strains for the two web Cs. One reason to explain this observation is that the
187 compression loading is only applied over the web area. The flanges are free from the
188 externally applied load and are only influenced by the composite action (force transfer) at the
189 rows of bolting. Another reason is found from analyzing the results of the Eigenvalue
190 buckling analysis as it shows SG7 and SG8 are positioned in a region with relative lower
191 flexure strains.
192 The specific lateral deformation curves plotted in Figure 5(b) for CFG1 test 3 shows that the
193 (negative) displacement measured by transducer [20] at $L/4$, *c.f.* with [19], was actually
194 picking-up a deflection from the pronounced development of a C-section flexural buckling
195 failure. In CFG1 test 1 (Figure 3(b)) and CFG1 test 2 (Figure 4(b)) the equivalent

displacements recorded by [19] at *L/2* and at *L/4* by [20] were registering a deformation for a failure by overall global (flexural) buckling. It is noted that flexural buckling of individual flange Cs is also being identified by the displacement measurements from transducer [18] at *L*/2.

It was found that the CFG1 columns in tests 1 and 2 ultimately failed by local crushing at one end. Photographs for this failure mechanism from tests 1 and 2 are given in Figures 9(a) and 9(b), respectively. It is noted that based on the ratio of cross-sectional areas the average stress over the web area (of 3000 mm^2) at rupture is 1.8 times the average stress given in Figure 3(a) and 4(a). Crushing was not the expected mode of ultimate failure and its existence in more than one specimen shows that load transfer into the ends of web was not uniform during testing. Such non-uniformity in the stress field from the presence of geometric imperfections (here from specimen and mounting fixtures on test machine) can be expected on site. It is important to recognize that design for member resistance based on assuming uniform stress could lead to a unsafe member that might fail with a mode not designed against.

From the strain gauges data reported in Figure 3(a) it is observed that the increased transversal stiffness in CFG1 test 1, guaranteed by having the $1/3^{rd}$ height bolting, has prevented an asymmetric distribution of the direct strain profiles in the two flanges of 9.5 and 6 mm thickness. It is found that there is strong evidence for a nearly uniform response in the full built-up section. A different strain distribution in the two flange thicknesses is observed in Figures 4(a) and 5(a) for tests 2 and 3. For these CFG1 columns there is a strain divergence within a group of three gauges of 60% in test 2 and 50% in test 3. This change in response is showing the presence, only in the thinner flange section, of second-order deformations. Taking the three strain readings from the thicker flange gauges it is seen that the difference is less, at 50% in test 2 and 25% in test 3.

The measured responses of the three CFG2 columns are presented in Figures 6 to 8. As seen from the curves plotted in Figures 6(a) and 7(a) there is a linearly increasing (uniform) stress at mid-height up to 40 kN (or 6 MPa). On further increasing compression the strain curves commence their divergence due to the non-linear response, and when one of the strain gauges recorded a tensile response it was signaling the onset of global (flexural) buckling. From measurements and visual inspection it is observed that, as a consequence of forces being transferred from the web Cs into the flanges through the bolting only at the ends, flexural deformation is induced in the flanges about the member's Major-axis plane and there is torsional deformation too. This form of buckling response was not seen in test 3. This CFG2 column was found to fail by local crushing at one end.

The reduced transversal stiffness in configuration CFG2, after removal of the bolting, allowed for the generation of flexural buckling and torsional deformations in both flanges. Evidence for this change in response from the CFG1 columns is seen by the higher divergence in the group of strain reading reported in part (a) of Figures 6 and 7.

Because there is a very noticeable reduction in column axial stiffness for CFG2 test 1 in Figure 6(b) and test 2 in Figure 7(b) when the load is above 40 kN the response has dramatically changed by the presence of flexural buckling of the individual flange Cs that are no longer connected to the web at the third-lengths.

COLUMN ANALYSIS

A preliminary evaluation of the resistances of the two column configurations was made using three different numerical approaches with the PFRP material taken to be linear elastic (Bank 2006). In what follows there is a presentation on using the Engesser (1889) closed form equation, and Eigenvalue (for bifurcation buckling) and geometrical non-linear finite element analyses. The latter analysis provided numerical stresses and displacements for a comparison

245 with the measured direct stress-lateral displacements via the strains measured by gauges SG1
246 and SG8 and the *y*-displacement from gauge [19].
247 Taking into account the shear deformability of FRP material the closed form equation to
248 predict the critical elastic (flexural) buckling resistance (P_{Esh}) is

249 $$P_{\text{Esh}} = \frac{\pi^2 E_z I_x}{\left(k^2 + u\right)\left(kL\right)^2} \quad . \tag{1}$$

250 In Equation (1), $E_z I_x$ is the flexural rigidity about the Minor-axis of deformation, k is the
251 effective length factor, and u is the shear flexibility parameter, given by $\frac{1}{A_{\text{s},x} G_{zx}} \frac{\pi^2 E_z I_x}{\left(kL\right)^2}$, with
252 $A_{\text{s},x} G_{zx}$ the member's shear rigidity. The Engesser's equation is a modification to the well-
253 known Euler formula that is for the shear rigid situation (i.e. when u is set to zero).
254 To calculate P_{Esh} the longitudinal modulus of elasticity (E_z) and in-plane shear modulus of
255 elasticity (G_{zx}) of the PFRP are taken from Table 2. These elastic constants are not measured
256 coupon values for the C-section in the testing programme. For this fact finding study the
257 authors decided to perform the analysis using the (lower) Design Manual values (Fiberline
258 2013) because this presented how the strut members were designed in the L'Aquila structure;
259 the only PFRP frame know with built-up members. The required geometric properties of A, I_x
260 and $A_{s,x}$ are those listed in Column (4) in Table 1. The effective length factor k is assumed to
261 be 1.0 to account for hinged ends in the columns having L = 2734 mm.
262 Two finite element models, using Ansys® software (Ansys 2011), were developed to simulate
263 the column configurations of CFG1 and CFG2. Salient information towards the finite element
264 (FE) modelling methodology is given next. A goal of the FE work was to obtain reliable
265 numerical results without recourse to needing a mesh possessing an excessive number of
266 degrees of freedom (d.o.f.). The FE mesh specification is shown in Figure 10. The *z*-axis
267 coincides with the member's longitudinal axis and the *x*-y plane is in the plane of the cross-

section. Flange and web Cs were meshed over their mid-plane surfaces by four-node quadrilateral shell elements. The shell element type was SHELL181, which can model the linear elastic response of orthotropic materials in thin-walled sections. Regions of shell elements to create the model were automatically meshed using the mapped meshing algorithm (Ansys 2011).

The bolted connections joining the four C sections were modelled by rigid beam elements of type BEAM188. They were manually assigned when building the mesh specification. At the two $1/3^{rd}$ lengths there were six bolts (see Figure 2(d)), with two in a vertical column to connect the back-to-back Cs forming the web. At the ends of the member there were only the four bolts that are used to join the four web flange outstands to the webs in the two Cs forming the flanges. The location of this bolting in the *x*-*y* plane is illustrated in Figure 2(a).

At the free ends the web (which extends beyond the free end of the flanges) was connected to a 'rigid' square plate that is perpendicular to the longitudinal axis of the member. To model the full specimen length of 2734 mm a rigid beam element, of length 45 mm is fixed to each plate and aligned with the member's z-axis. The mesh specification had been formulated in such a way to ensure that nodal locations corresponded exactly to bolt hole positions and to where the displacement transducers are located.

Nodal d.o.f. at the end of the 'extension' beams were restrained in a way that models the two hinges found in the experimental set-up illustrated in Figure 2. At the extreme ends, where the compressive load was applied, the translational d.o.f.s in the *x*-direction and *y*-direction and the rotation degree of freedom around the *z*-axis were restrained. Applied in the *z*-direction, for the initial load factor, is a unit (compressive) load of 1 kN. At the other end of the column model the translational degree of freedom in the *z*-direction was also fully restrained to complete the displacement boundary conditions.

292 The linear elastic FRP is taken to be transversely isotropic (i.e. the behaviour is the same in
293 the *x*- and *y*-directions), with the orthotropic elastic constants listed in Column (3) of Table 2.
294 Notation for the elastic constants in Column (1) is given in Column (2).
295 The Eigenvalue solution was carried out using the block Lanczos algorithm (Ansys 2011).
296 For the two simulations of CFG1 and CFG2 the first buckling mode results were extracted.
297 For column-type CFG1 the predicted critical elastic buckling is 230 kN. The buckled (mode)
298 shape is shown in Figure 11 by way of a contour plot along the length of the column for the
299 nodal displacements in the *y*-direction. The first (Eigenvalue) mode is characterized by
300 Minor-axis global (flexural) buckling of the flanges, accompanied by global flexural buckling
301 of the web C-sections between the bolt rows. Because a bifurcation analysis has been carried
302 out the numerical displacements do not represent the actual test displacements. The contour
303 plots presented in the three figures do allow a qualitative understanding towards the overall
304 buckling response of the built-up member with composite action from bolting at the third
305 lengths.
306 For configuration CFG2 (without bolting at the $1/3^{rd}$ and $2/3^{rd}$ lengths) the predicted critical
307 buckling load is much lower at 39 kN. The buckled shape is illustrated in Fig. 12(a) and, as
308 expected, it is dominated by flexural buckling of the thinner (6.5 mm) flange C section. At
309 17% of the CFG1 bifurcation load the significantly lower resistance has to be due to the
310 removal of the very beneficial influence of the composite action from having bolting at the
311 two $1/3^{rd}$ length levels in CFG1. The CFG2 bolting detailing has therefore been shown to
312 have increased the buckling length of a flange C-section for flexural buckling failure to occur
313 first, and at a compression force that is five times lower than measured in CFG1 test 3 (see
314 Fig. 5).
315 Parts (b) and (c) of Fig. 12 present the Eigenvalue second and third mode shapes for CFG2,
316 with contour plotting for the *x*- and *y*-displacement, respectively. The relevance of presenting

317 the higher mode shapes is that they are used to define the geometric imperfections and an
318 essential contact pairing (restraining C-section separation) in the modelling methodology for
319 the non-linear FE simulations to follow.
320 A geometric non-linear FEA was also conducted in order to better understand the response of
321 the two column configurations over the loading range. The basic FE model was the same
322 described for the Eigenvalue analysis. For the non-linear analysis the compressive load was
323 applied at one end of the model through consecutive steps. The analysis was performed by
324 applying the automatic load stepping option that enables ANSYS® to choose the non-linear
325 solution options, such as: the type of equation solver, the Newton-Raphson solution options,
326 the convergence criteria, the maximum number of iterations. Because the choice of these
327 options influences the speed and numerical precision of the computational solution it was a
328 prudent modeling decision to let the code decide the progression of the non-linear analysis to
329 a buckling mode of failure.
330 In order to execute the non-linear analysis, geometric imperfections were generated
331 consistently with the experimentally observed buckled shapes reproduced in the Eigenvalue
332 analysis. Imperfections are automatically generated by ANSYS® updating the geometry of
333 the FE mesh as a function of a scaling factor related to the mode shapes selected from those
334 computed and illustrated in Figs. 11 and 12. For the generic scaling factor, given notation *s*,
335 the FE modeling geometry is updated in such a way to have a maximum value of the
336 geometric imperfection equal to *s* (in the units for the FE mesh), where the position for the
337 maximum amplitude was established from the Eignevalue analysis mode shape.
338 For CFG1 it was recognized that the first mode shape, illustrated in Fig. 11, matched the one
339 experimentally observed. Imperfections were then generated on the base of this mode shape,
340 with three scaling factors (*s*) set at 1 mm, 2.5 mm and 5 mm. The deformed shape at the last
341 load step from the non-linear analysis is represented in Fig. 13 by a contour plot for the *y*-

displacements. It is observed that the deformed shape is similar to the first mode shape in Fig. 11, calculated by the Eigenvalue analysis. The predicted ultimate load is found to be 178 to 213 kN, depending on the scaling factor *s*; the higher the value of s the lower the resistance of the built-up column is. The failure load was taken as the load in the numerical solution when there was a loss of static equilibrium and an absence of convergence at the next load step.

From column-type CFG2 the mode shapes of interest to define the geometric imperfections were the first and third. These modes from the Eigenvalue analysis are illustrated in Parts (a) and (c) of Fig. 12. The second mode shape, shown in Fig. 12(b), cannot be physically activated because of the mechanical interaction (for the composite action) between the flange and the web prevents an inner (towards the web) deflection of the 9.5 mm thick flange channel. In order to eliminate any activation of the second mode shape contact pairs between the thicker flange of 9.5 mm thickness and the 6.5 mm web Cs are introduced along the full column height. This FE modeling feature is shown in Figure 14. Since a gap is present in the FE mesh between web and flanges (because shell elements are located at the mid-surfaces of their thin-walls) the "close initial gap" option is activated for contact modeling (Ansys 2011).

In order to activate the first buckling mode in the non-linear analysis with CFG2 it was necessary to apply the geometric imperfection defining this mode shape with *s* equal to 5 mm. Three scaling factors of *s* = 1 mm, 2.5 mm and 5 mm were employed for the equivalent imperfection associated with the third mode shape, as shown in Fig. 12(c).

The deformed shape at the last load step is represented in Fig. 15, together with a contour plot of the displacements in the *x*-direction (left-sided) and *y*-direction (right-sided). The deformed shape is characterized by lateral deformation of the thinner (6.5 mm) flange in the *x*-direction and of the web in the *y*-direction. The ultimate load is found to be 45 to 56 kN, depending on the scaling factor *s* chosen for the third mode shape; again, the larger *s* is the lower is the resistance.

Comparison between numerical and test results

Table 3 is used to make a comparison between the experimental and numerical determined resistances of columns CFG1 and CFG2. Column (1) gives the label for the six specimens and Column (2) reports their ultimate test load, and when occurring their buckling load, which is given between parentheses. Columns (3) and (4) give the flexural buckling resistance as determined by the Euler and Engesser closed form equations, respectively. By including shear deformation, P_{Esh} (from Equation (1)) is about 5% lower; a similar percentage reduction with concentrically loaded pultruded columns of H-shapes has been established by Mottram *et al*. (2003). Columns (5) and (6) present the bifurcation and non-linear FEA results employing the modelling methodology introduced above. Section properties are taken from Table 1 and the elastic constants are from Table 2 (they were not determined using coupons cut from the C sections in the built-up specimens).

A form of buckling failure was not realised with configuration CFG1 in tests 1 and 2. The experimental ultimate loads of 148 kN and 249 kN were established by local compressive crushing of the web at one end. The considerable difference of 68% (or 101 kN) is solely due to the technical challenge of ensuring there is a uniform distribution of the load over the web's total area of 3000 mm^2. A possible reason for why the failure load in test 2 exceeded the upper bound Eigenvalue buckling load of 230 kN is that the shape of the out-of-straightness imperfection for Minor-axis flexural buckling at the beginning of testing was for a higher mode. Supporting this proposal is the similar experimental response reported from test number 11 (H-profile of 152x152x9.53 mm at length 3300 mm) in the series of concentrically loaded column tests by Mottram *et al*. (2003).

The ultimate and buckling load of 193 kN from CFG1 test 3 is seen to be 85% of the critical load of 230 kN by the Eigenvalue FEA. A higher critical elastic buckling load is to be

392 expected from an Eigenvalue analysis because the influence of the imperfections present in
393 testing will ensure the measured resistance is lower, if not significantly so. It is observed that
394 the buckling shape established in the FEA and presented in Fig. 11 is found to correspond to
395 that visually observed in CFG1 test 3.
396 It is found that the FEA bifurcation load is 70% of the Engesser flexural buckling resistance
397 of 331 kN. This latter is computed under the hypothesis of full composite action, whereas the
398 degree of mechanical interaction between the four channels is taken into account in the FE
399 analysis, leading to a lower buckling load that is found to be closer to the experimental
400 buckling load. This finding suggests that FEA is required to establish the buckling resistance
401 of built-up compression struts when the degree of composite action between individual
402 sections has a significant role in controlling structural performance.
403 In Fig. 16 the test data from CFG1 tests 1 to 3 for the *y*-displacement at mid-height is
404 compared with the equivalent non-linear prediction for a compressive force to ultimate
405 failure. Unfilled symbols are for experimental results (square for test 1, triangle for test 2 and
406 rhombus for test 3), while filled symbols are for FE results (square for s = 1 mm, triangle for
407 s = 2.5 mm and rhombus for s = 5 mm). For the FEA curves the three scaling factors are for
408 the imposed geometric imperfections in mesh specification. It can be seen that the range of s
409 values is able to simulate reasonably well the non-linear stiffness behaviour; it is noted that
410 each specimen needs a different s and crushing failure is not captured.
411 Let's now consider the same comparison for column configuration CFG2. From testing it was
412 found that a form of buckling failure was not achieved in test 3. The bifurcation load of 39
413 kN in Column (5) of Table 3 is seen to be within 1 kN of the experimental ultimate load
414 achieved in the other two tests. For CFG2 tests 1 and 2 the load-axial displacement curves in
415 Figs. 6 and 7 show that there was a stable post-buckling branch. The FEA predicted buckling
416 shape shown in Fig. 15 is similar to that visually observed in these two tests.

In Fig. 17 the test results for column configuration CFG2 are compared with the non-linear FEA outputs. The format of the figure is the same as in Fig. 16 for the CFG1 columns, except that the three scaling factors (i.e. *s* set at 1 mm, 2.5 mm or 5 mm) are for the third buckling mode shape (see Fig. 12(c)). A constant scaling factor of 5 mm was applied to the geometric imperfection of a half sine wave along the column length for the first mode shape. It can be seen that with scaling factors of 1 and 2.5 mm with the third mode the computational curves tend to fit the measured response of test 2. Modelling requires *s* to be set to 5 mm for the FEA curve to correspond to what was found in test 1.

CONCLUDING REMARKS

A fact finding study has been made on the structural response of a built-up column (envelop is 152 x 171 mm) of length 2.734 m subjected to (concentric) compressive loading. To understand the behavior the study combined physical testing and (linear elastic material) numerical approaches. Mechanical performances from three columns, for the configuration that is similar to the strut members in the FRP structure inside the church of Santa Maria Paganica in L'Aquila, were found to be dependent on the end boundary conditions. Two of these specimens ultimately failed at one end, by material crushing in the two channel sections forming the web (there is no loading applied into the two flange channel sections). This result was not expected *a proiri*, and its presence highlights the sensitive of FRP materials to localized failure where concentrated forces are transferred into (and out of) members.

In a third test the mode of failure was by global flexural buckling when the compression force was 193 kN. Numerical predictions of 230 kN by Eigenvalue FEA and 331 kN from the Engesser closed form equation were much higher; even when the moduli of elasticity where design manual value that are known to be lower than actual. This finding suggests that there is not full composite action between the four channel sections, and opens up the possibility

that with additional bolting, say at the sixth length locations, the column buckling strength can be further enhanced. Moreover, by combining experimental and numerical results it is observed that imperfections, geometric and from other sources, have an important role in establishing the structural performance of the built-up columns.

From non-linear FEA the ultimate compressive load was in the range 178 to 213 kN depending on the magnitude of the scaling factor in the FE modelling used to define the amplitude of geometric imperfections. This was found to bound the measured buckling resistance from test 3. In the FE modelling it was found that by increasing the scaling factor from 1 to 5 mm there was a decrease in both critical elastic buckling load and the members' initial axial stiffness. A numerical prediction was observed to be close to what was measured when the scaling factor was either 2.5 or 5 mm. The initial stiffness was found to be underestimated by FEA, unless the lowest geometric imperfection scaling factor of 1 mm was applied. It was established that the computed buckled shape corresponds to that visually observed in test 3.

By removing the two rows of bolted connections at the third lengths the much lower column resistance of about 40 kN was determined in two of the three tests with this column configuration. Material crushing at one end was one reason why the three nominally identical columns failed differently. A critical elastic buckling load of 39 kN was predicted by Eigenvalue FEA. It can be concluded that the bolting at third lengths was sufficient, and necessary, for the built-up member to have column strength that was five times higher than if the built-up strut is without the composite action. The largest scaling factor of 5 mm for the first mode shape was found to be the 'lowest' that would activated this mode in the non-linear FEA.

A reasonable, but not good, agreement between the equivalent numerical and the experimental results was observed prior to the first non-linear branch and before buckling

467 deformation occurred. The post-buckling stage that followed in testing had a stable branch
468 that cannot be reliably simulated by FEA. Up to a mid-height lateral displacement of 13 mm
469 (or 1/200 of column height) there was little difference between FEA and testing for flexure
470 occurring about the minor-axis. Continuing to increasing load it was found that the deviation
471 in load-displacement response between the test columns in a group of three may become very
472 significant. The numerical-experimental comparison reported in this paper has shown that the
473 response of built-up FRP members could be challenging to reliably predict by FEA.
474

475 **REFERENCES**

476 Anonymous (2011). *ANSYS® Multiphysics, Release 14.0, Help System*, ANSYS Inc.

477 Bank, L. C. (2006). *Composites for Construction - Structural Design with FRP Materials*,
478 John Wiley & Sons, N.J.

479 Barbero, E. J., Dede, E. K., Jones, S. (2000). "Experimental Verification of Buckling-mode
480 Interaction in Intermediate-length Composite Columns", *International Journal of Solids and*
481 *Structures*, 37(29), 3919-3934.

482 Boscato, G. and Russo, S. (2009). "Free Vibrations of Pultruded FRP Elements: Mechanical
483 Characterization, Analysis, and Applications", *Journal of Composite for Construction*,
484 ASCE, 13(6), 565-574.

485 Boscato, G., Mottram, J., Russo, S. (2011). "Dynamic Response of a Sheet Pile of Fiber-
486 Reinforced Polymer for Waterfront Barriers", *Journal of Composite for Construction*, ASCE,
487 15(6), 974–984.

488 Di Tommaso, A. and Russo, S. (2003). "Shape Influence in Buckling of GFRP Pultruded
489 Columns", *Mechanics of Composite Materials*, 39(4), 329-340.

490 Engesser, F. (1889). "Ueber die Knickfestigkeit gerader Stabe", *Zeitschrift für Architekter*
491 *und Ingenieurwsen*, 35(4), 455-462 (in German).

492 Fiberline design manual for structural profiles in composite materials. (2013). *Fiberline*
493 *Composites A/S*, Kolding, Denmark.
494 Hashem, Z. A. and Yuan, R. L. (2001), "Short vs. Long Column Behavior of Pultruded
495 Glass-fiber Reinforced Polymer Composites", *Construction and Building Materials*, 15(8),
496 369-378.
497 Lane, A. and Mottram, J.T. (2002). "The Influence of Modal Coupling upon the Buckling of
498 Concentrically Pultruded Fibre-reinforced Plastic Columns", *Proceedings of the Institution of*
499 *Mechanical Engineers Part L: J. Materials - Design and Applications*, 216 133-144.
500 Mottram, J. T. (2004). "Determination of Critical Load for Flange Buckling in Concentrically
501 Loaded Pultruded Columns", *Composites*: *Part B Engineering*, 35 35-47.
502 Mottram, J. T. (2011). "Does Performance Based Design with Fibre Reinforced Polymer
503 Components and Structures Provide any new Benefits and Challenges?", *The Structural*
504 *Engineer*, 89(6), 23-27.
505 Mottram, J. T., Brown, N. D. and Anderson, D. (2003). "Physical Testing for Concentrically
506 Loaded Columns of Pultruded Glass Fibre Reinforced Plastic Profile", *Structures and*
507 *Buildings*, 156(2), 205-219.
508 Pecce, M. and Cosenza, E. (2000). "Local Buckling Curves for the Design of FRP Profiles",
509 *Thin-Walled Structures*, 37(3), 207-222.
510 Russo, S. (2012). "Experimental and Finite Element Analysis of a Very Large Pultruded FRP
511 Structure Subjected to Free Vibration", *Composite Structures*, 94(3), 1097-1105.
512 Russo, S. (2007). Strutture in Composito: Sperimentazione, Teoria e Applicazioni, Edited by
513 Ulrico Hoepli, Milano, Italy (in Italian).
514 Russo, S., Boscato, G. and Mottram, J. T. (2012). "Design and Free Vibrations of a Large
515 Temporary Roof FRP structure for the Santa Maria Paganica Church in L'Aquila, Italy".

Presented at *6th International Conference on FRP Composites in Civil Engineering (CICE 2012)*, Section 8: All-FRP and Smart FRP Structures, Paper 209, 13th-15th June 2012.

Turvey, G. J. and Zhang, Y. (2006). "A Computational and Experimental Analysis of the Buckling, Postbuckling and Initial Failure of Pultruded GRP Columns", *Computers and Structures*, 84(22-23), 1527-1537.

Table 1. Physical and geometric properties of four channel profiles.

Property (1)	Notation (2)	Value	
		Nominal (3)	Exp. (4)
Cross-sectional area of column	A	83.2 cm^2	65.8 cm^2
Minor-axis second moment of area	I_x	1370 cm^4	1250 cm^4
Major-axis second moment of area	I_y	3550 cm^4	2840 cm^4
Minor-axis shear area	$A_{s,x}$	37.1 cm^2	26.6 cm^2
Major-axis shear area	$A_{s,y}$	47.7 cm^2	38.6 cm^2
Bulk weight density of FRP		1850 kg/m^3	
Volume fraction of E-glass fibre		48%	

Table 2. Elastic constants for the C-shape section (Fiberline 2013).

Definition (1)	Notation (2)	Value (3)
Longitudinal modulus of elasticity	E_z	23 GPa
Transverse modulus of elasticity	$E_x = E_y$	8.5 GPa
Transverse shear modulus of elasticity	G_{xy}	3.4 GPa
In-plane shear modulus of elasticity	$G_{zx} = G_{zy}$	3 GPa
Major Poisson's ratio	$\nu_{zx} = \nu_{zy}$	0.23
Minor Poisson's ratio	ν_{xy}	0.09

533 Table 3. Ultimate test loads and numerical elastic loads.

Column specimen (1)	Ultimate test load (buckling load) [kN] (2)	Flexural buckling load from Euler $P_E = \frac{\pi^2 EI}{(kl)^2}$ [kN] (3)	P_{Esh} Equ. (1) [kN] (4)	Eigenvalue buckling load [kN] (5)	Non-linear FEA ultimate load [kN] (6)
CFG1 test 1	148	349	331	230	178-213
CFG1 test 2	249				
CFG1 test 3	193 (193)				
CFG2 test 1	123 (40)			39	46-56
CFG2 test 2	118 (40)				
CFG2 test 3	122				

534

535

Figure 1. Temporary FRP structure for Santa Maria Paganica church: (a) overall construction; (b) details of bolted gusset plate for frame joints.

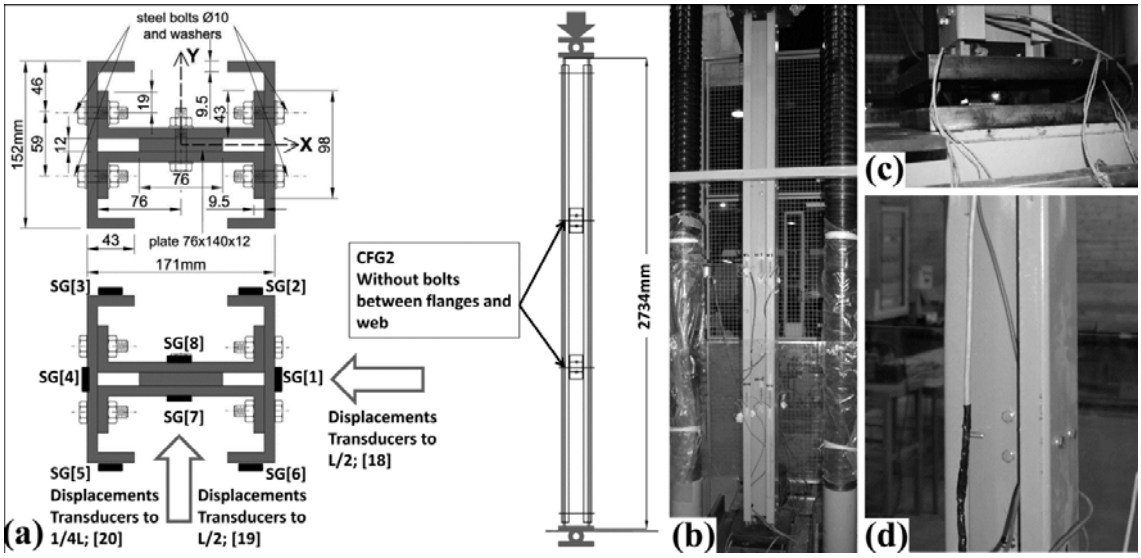

Figure 2. Details of PFRP built-up columns: (a) member cross-section and scheme for column testing; (b) actual test set-up; (c) detail of hinge end constraints; (d) M10 steel bolting for composite action between the four C-sections.

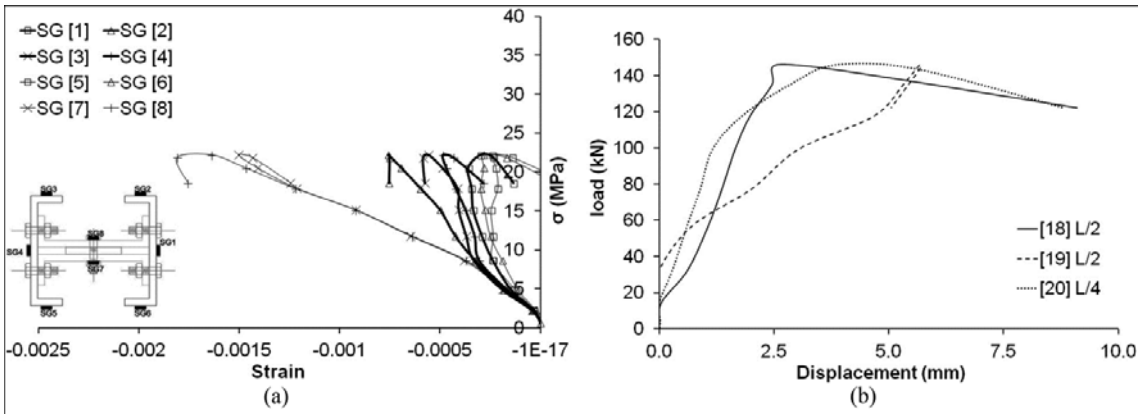

Figure 3. CFG1 test 1: (a) eight direct stress-direct strain curves; (b) three load-lateral displacement curves.

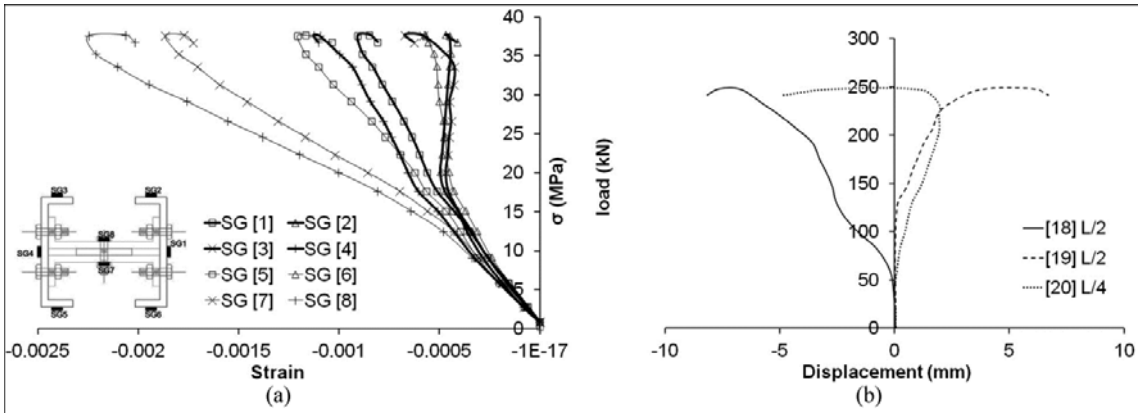

Figure 4. CFG1 test 2: a) eight direct stress-direct strain curves; (b) three load-lateral displacement curves.

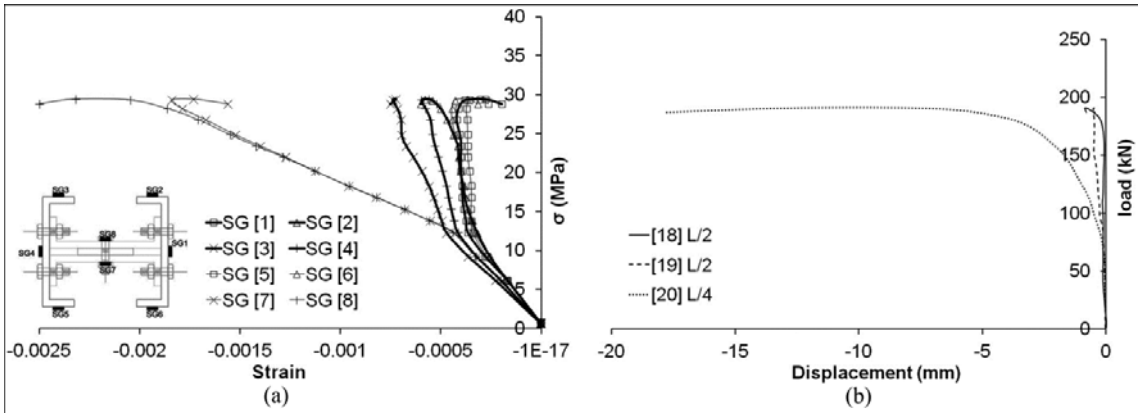

Figure 5. CFG1 test 3: a) eight direct stress-direct strain curves; (b) three load-lateral displacement curves.

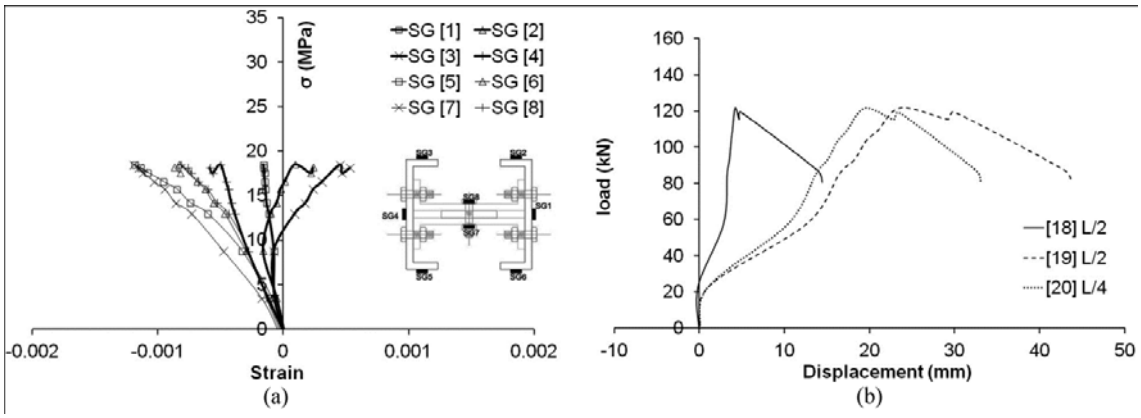

Figure 6. CFG2 test 1: a) eight direct stress-direct strain curves; (b) three load-lateral displacement curves.

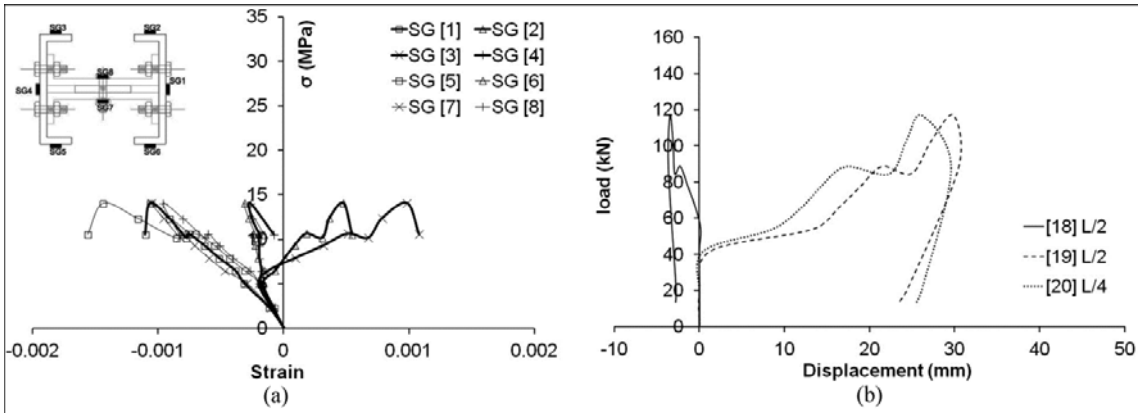

Figure 7. CFG2 test 2: a) eight direct stress-direct strain curves; (b) three load-lateral displacement curves.

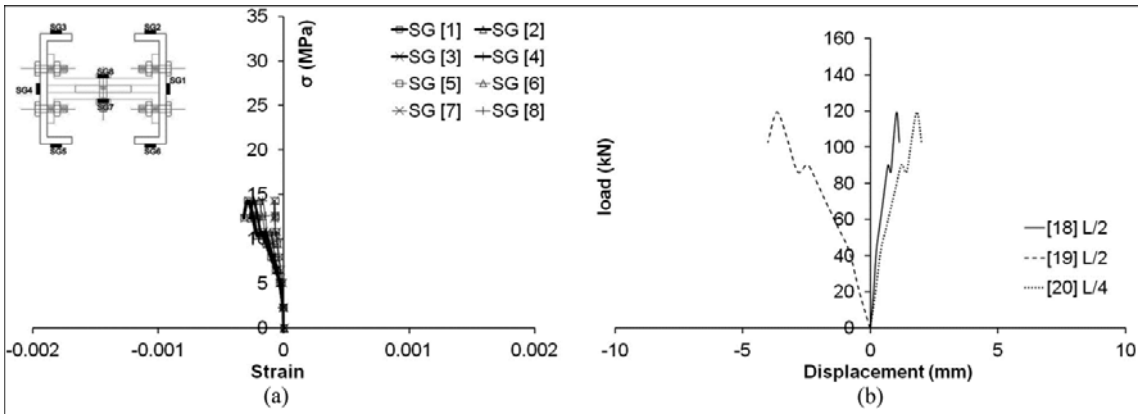

Figure 8. CFG2 test 3: a) eight direct stress-direct strain curves; (b) three load-lateral displacement curves.

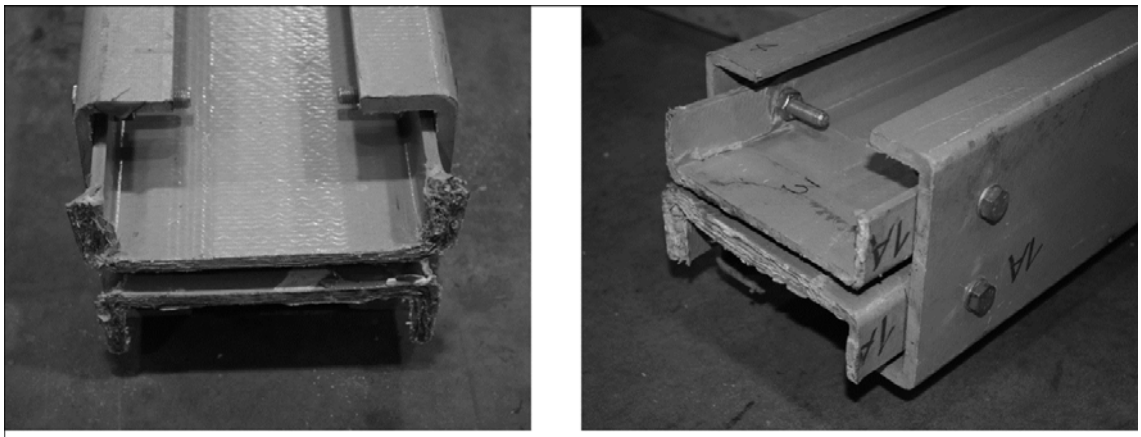

Figure 9. Local end-crushing in column-type CFG1: (a) test 1; (b) test 2.

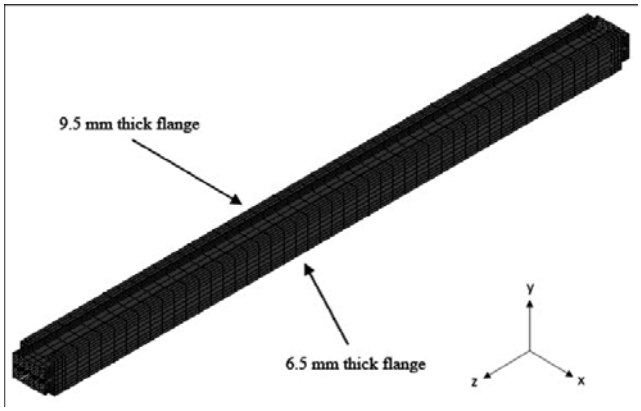

Figure 10. Isometric view of finite elements mesh for built-up column defined in Figure 2.

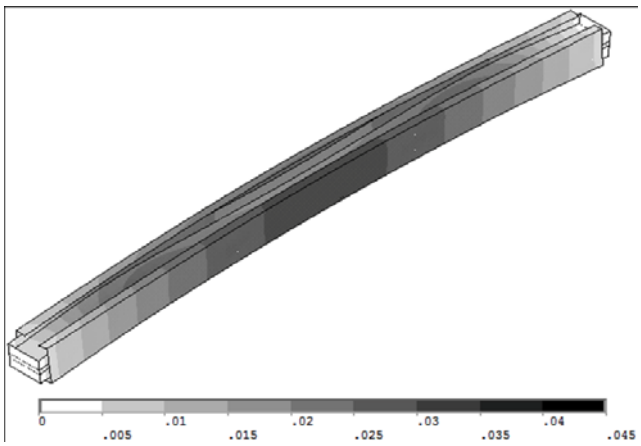

Figure 11. Eigenvalue first mode shape with contour plot for lateral *y*-displacement for column configuration CFG1.

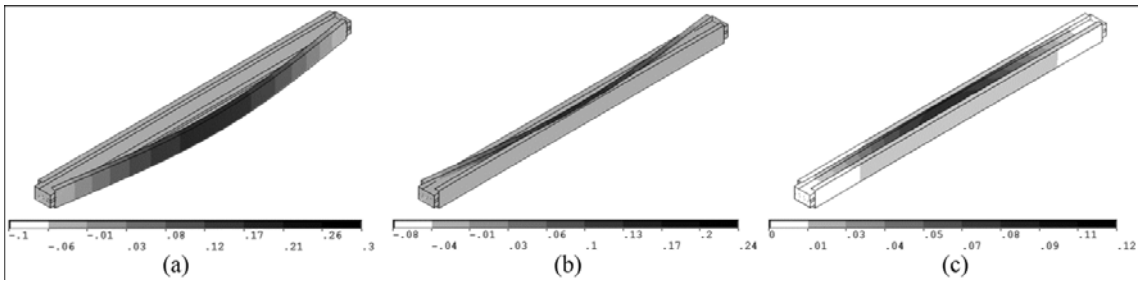

Figure 12. Eigenvalue first mode shape (a), second mode shape (b) and third mode shape (c) with contour plot for lateral *x*-displacement (a-b) and *y*-displacement (c) for column configuration CFG2.

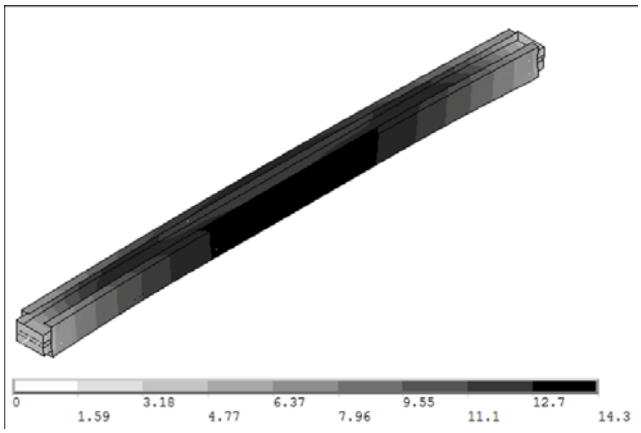

Figure 13. Non-linear FEA deformed shape via lateral *y*-displacement (mm) for configuration CFG1.

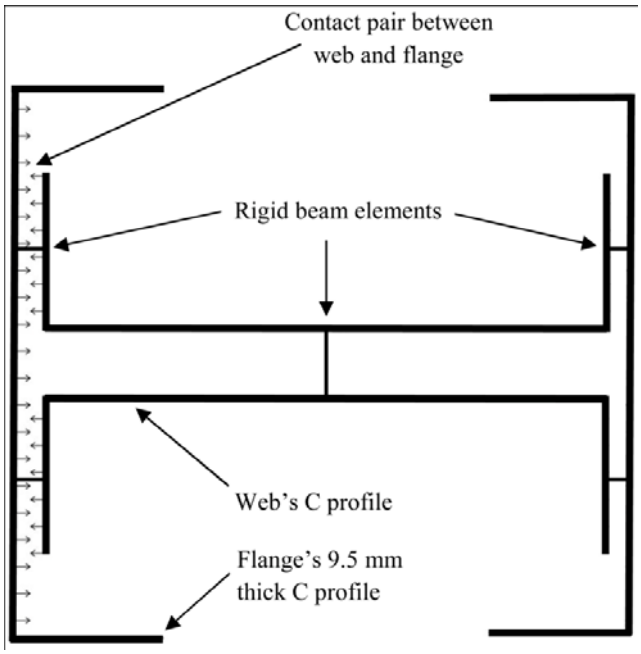

Figure 14. Locations for contact pairs between web and flange and for rigid-beam elements for the bolted connections when modelling column-type CFG2.

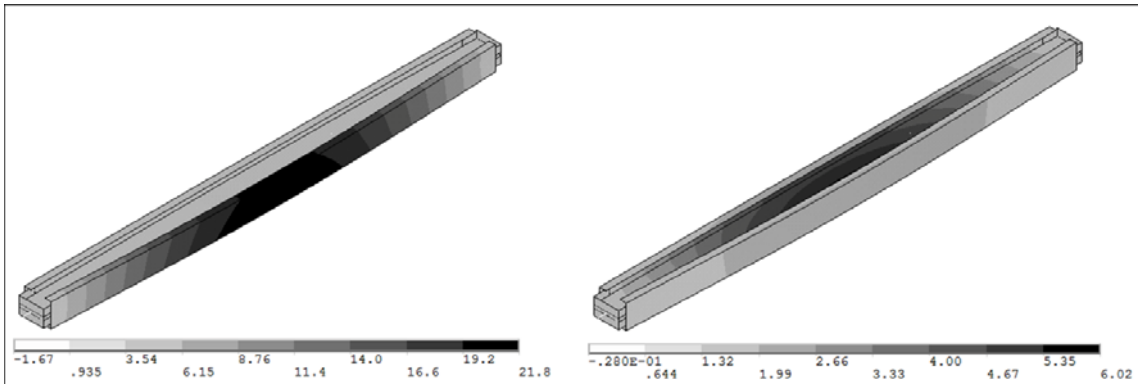

Figure 15. Non-linear FEA deformed shape using lateral *x*-displacment (left) and y-displacement (mm) (right) for configuration CFG2.

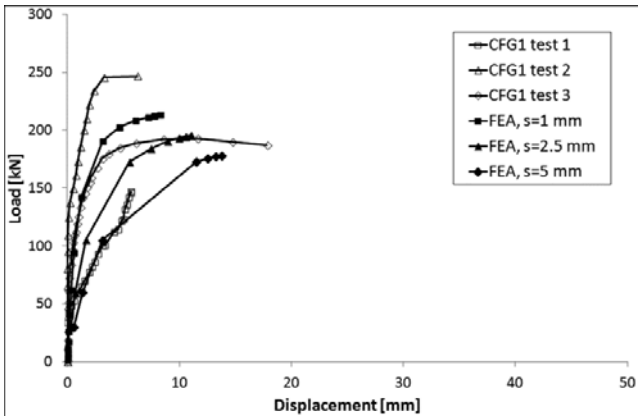

Figure 16. Experimental and non-linear FEA *y*-displacements with compression force at mid-height for CFG1. FEA results with three factors *s* for the geometric imperfection for the first mode shape.

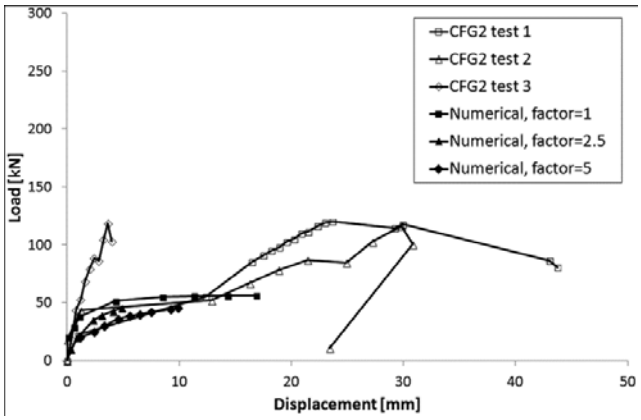

Figure 17. Experimental and non-linear FEA lateral *y*-displacements with compressive load for CFG2 at mid-height. FEA results with three factors *s* for the geometric imperfection for the third mode shape.